



Reactivity of Antimony Oxides and MSb₂O₆ (M = Cu, Ni, Co), Trirutile-type Phases with Metallic Lithium

D. Larcher,^{a,z} A. S. Prakash,^a L. Laffont,^a M. Womes,^b J. C. Jumas,^b
J. Olivier-Fourcade,^b M. S. Hedge,^c and J.-M. Tarascon^{a,*}

^aLaboratoire de Réactivité et Chimie des Solides, Université de Picardie Jules Verne, 80039 Amiens, France

^bLaboratoire des Agrégats Moléculaires et Matériaux Inorganiques, Université Montpellier II, France

^cSolid State and Structural Chemistry Unit, Indian Institute of Science, Bangalore, India, 560 012

Isostructural MSb₂O₆ (M = Cu, Ni, Co) trirutile-type phases were prepared by solid-state synthesis and their electrochemical activity towards lithium was investigated. NiSb₂O₆ and CoSb₂O₆ showed similar electrochemical behavior, with an uptake of about 18–19 Li per formula unit along the first reduction and only 6–7 Li reversibly removed upon subsequent cycling. This totally differs from the behavior of CuSb₂O₆ that was found to react with only about 7 Li during the first reduction, without any capacity recovered on subsequent charge. From X-ray diffraction data, both Cu and Co phases lead to an amorphous composite down to 0 V. From high-resolution transmission electron microscopy observations, reduced CoSb₂O₆ consists of 10–50 nm Co particles dispersed in a Li₃Sb + Li₂O matrix. For CuSb₂O₆, our results and observations enlightened a two-step reduction: First, the formation of Cu clusters through an electrochemically-driven exchange reaction leading to Li₂Sb₂O₆, and then reduction of this matrix into 5 nm Sb domains dispersed in an insulating amorphous Li-rich Li–Sb^V–O matrix, preventing any further alloying reaction and any charge reaction. The complete charge irreversibility observed on Li/Sb₂O₅ half-cells confirmed this point, while the Li reduction of Sb₂O₃ emphasized a close similarity with the reactivity of the (Ni/Co)Sb₂O₆ phases, suggesting a first reduction step of Sb⁵⁺ into Sb³⁺, assuring conduction and subsequent cycling capacity. Despite the composite nature of the as-formed electrode and the very fine Sb particles, the reversibility of the alloying reaction was not found to be satisfactory for Li-ion cells.

© 2006 The Electrochemical Society. [DOI: 10.1149/1.2219711] All rights reserved.

Manuscript received March 14, 2006. Available electronically July 21, 2006.

Rechargeable lithium-ion batteries, first introduced in 1990, are presently powering most of the portable electronic devices. In the continuing endeavor to improve these systems, researchers have shared their efforts between optimizing electrode materials reacting with Li through the classical Li insertion/deinsertion mechanism and searching for electrode materials displaying new reversible Li reactivity mechanisms. Pursuing the latter path, it was recently shown that, when working at the nanometer scale, Li electrochemically driven conversion reactions (oxides ⇌ metals) can be achieved and maintained for hundreds of cycles. Moreover, depending on the oxidation state of the 3d-metal, these conversion reactions can either involve 1 (Cu₂O), 2 (FeO, NiO, CoO, CuO), 2.66 (Co₃O₄),¹ 3 (Fe₂O₃),² or 4 (RuO₂)³ electrons, thus offering the possibility of having compounds with large capacities as compared to only 0.5 Li per metal in today's manufactured intercalation materials. Soon after, many other sightings of conversion reactions processes in nitride,⁴ fluoride,⁵ phosphide,⁶ or sulfide⁷ compounds were reported to occur at potentials ranging from 0 to 3.0 V vs Li⁺/Li⁰, depending on the nature of the anion. Along that line, we decided to study the electrochemical properties of compounds containing metal elements with even higher oxidation states, and therefore decided to focus on Sb^V-based oxides and more specifically on the trirutile-type compounds of general formula M^{+II}Sb₂^VO₆, whose structure derives from the rutile lattice by tripling the c-axis.⁸ Besides their ability to exist under high oxidation state, our choice for Sb is also nested in its ability to alloy with Li leading to Li₃Sb,⁹ therefore potentially offering an uptake of 8 Li per Sb^V via both conversion and alloying.

In the present study, we prepare cobalt, copper, and nickel-containing trirutile materials and compare their respective reactivity and reversibility through electrochemical titration, Mössbauer effect (ME) and electron dispersive X-ray (EDXS) spectroscopies, combined with ex situ and in situ X-ray diffraction (XRD) and high-resolution transmission electron microscopy (HRTEM). For comparison purposes and for the sake of references, the same set of

investigation tools are also applied to Li₂Sb₂O₆ ternary phase as well as to binary oxides containing either Sb^V (Sb₂O₃), Sb^{III} (Senarmontite, Sb₂O₃), or a mixture of Sb^V and Sb^{III} (Cervantite, Sb₂O₄).¹⁰ That way, we propose reaction mechanisms aimed at understanding the drastic differences in electrochemical responses for CuSb₂O₆ and Li–(Sb^V–O) phases on the one hand, and for (Co/Ni)Sb₂O₆ and trivalent binary oxides on the other hand.

Experimental

Samples syntheses.—MSb₂O₆ (M = Cu, Ni, and Co) metal antimonates were synthesized by solid-state reaction from a stoichiometric mixture of MO (M = Cu, Ni, or Co) and Sb₂O₅ powders (Aldrich, purities >99.9%). The mixtures were air-heated in an alumina crucible at 800°C for 2–3 days with intermediate grindings. Afterwards, the sample was cooled down to room temperature and ground to obtain fine powder. Phase purity and composition of purchased Sb₂O₃ (Senarmontite) and Sb (Fluka, purity >99.5%) were checked by XRD and Mössbauer spectroscopy, respectively. The batch of Sb₂O₅ was found badly crystallized but thermal analysis (TGA) coupled with Mössbauer spectroscopy ascertained the formula Sb₂O₅·0.4 H₂O.

Powdered Li₂Sb₂O₃ was synthesized by reacting Li₂CO₃ (Aldrich, >99.9%) with Sb₂O₃ under static air at 750°C for 24 h with a heating rate of 5°/min. A slight excess of Li salt was necessary to compensate heating-induced loss.

Partially reduced α-Sb₂O₄ (Cervantite) was synthesized by one-step heating of a batch of Sb₂O₅·0.4 H₂O under static air at a rate of 5°C/min up to 800°C.¹¹

Characterization.—Routine phase composition of powders was achieved by XRD using a Philips diffractometer (PW 1710, Cu Kα radiation, λ = 1.5418 Å) equipped with back monochromator. Lattice parameters were refined using the Fullprof refinement software.¹²

The electrochemical reactivity of MSb₂O₆ (M = Cu, Ni, Co), Sb oxides and Sb, toward Li was performed in Swagelok cells assembled in an argon-filled MBraun MB150B-G dry box. The positive electrode composite, consisting of 85 wt % of active material and 15 wt % of conducting SP carbon, was separated from the nega-

* Electrochemical Society Active Member.

^z Corresponding author: Dominique.Larcher@sc.u-picardie.fr

tive electrode (lithium foil) by two sheets of Whatman GF/D borosilicate fiber glass, the assembly being soaked by a 1 M solution of LiPF_6 in an ethylene carbonate (EC)/dimethyl carbonate (DMC) solvent mixture (1:1 v/v). Typically, the cells were cycled at 20°C in a galvanostatic mode between 0 and 2–3 V vs $\text{Li}^+/\text{Li}^\circ$ using a Mac-Pile automatic cycling data recording system (Biologic SA Claix, France) and at rates ranging from 1 Li in 5 h (noted C/5) to 1 Li in 20 h (noted C/20). Galvanostatic intermittent titration technique (GITT) experiment was also performed to determine the quasiequilibrium open-circuit potential at various reaction levels. The open-circuit voltage (OCV) was determined once the voltage evolution remained under 3 mV/h, after reduction steps of 2 h at a C/10 rate (i.e., 0.2 Li per step). Based on the high gravimetric capacities released by the tested samples, the contribution of the added SP carbon (60 mAh/g) onto the cells capacities is neglected.

The structural evolution of the electrode material during electrochemical reactions was monitored using in situ XRD measurements. To carry out such an experiment, a home-designed XRD electrochemical cell¹³ was equipped with a Be window being transparent to the X-rays while acting as a current collector. This cell was then placed in a Scintag diffractometer (Cu $K\alpha$, $\lambda = 1.5418 \text{ \AA}$), and XRD scans were collected as cell is cycled at a constant current rate as low as 1 Li in 20 h.

Mössbauer and HRTEM ex situ measurements were performed on the electrodes at several depths of discharge and charge. In order to remove adsorbed species and soaking residual electrolyte, the Swagelok cells were opened inside the glove box and the powders washed several times with salt-free solvent and separated from the liquid by centrifugation.

The ^{121}Sb Mössbauer spectra were obtained with a classical EG & G constant acceleration spectrometer in transmission mode. The source of nominal activity 0.5 mCi was ^{121m}Sn in a BaSnO_3 matrix. During the measurements, both source and absorbers were simultaneously cooled down to 4 K in order to increase the fraction of recoil-free absorption and emission processes. The active material was placed on a specific sample holder transparent to the γ -rays. The velocity scale was calibrated with the standard spectrum of an iron absorber using a $^{57}\text{Co}(\text{Rh})$ source. The zero isomer shift was defined from the spectrum of InSb at 4 K [$\delta = -8.70(4) \text{ mm/s}$ relative to the $\text{Ba}^{121m}\text{SnO}_3$ source]. The data was processed using a transmission integral analysis software GM5SIT¹⁴ with the Mössbauer source fraction (fs) and source line width (Γ_s) held constant at 0.62 and 1.45 mm/s, respectively.

TEM and HRTEM imaging were performed using a FEI TECNAI F20 S-TWIN equipped with an EDXS detector. Ground samples were deposited on copper or nickel grids coated with lacey-carbon films. For sensitive-reduced materials, these preparations were done within the argon-filled dry box. The diffraction patterns were obtained in selected area diffraction (SAED) mode or by Fourier transform of the HRTEM imaging. The SAED patterns obtained on polycrystalline samples were analyzed using the process diffraction software.¹⁵

Results and discussions

The XRD patterns of CuSb_2O_6 , CoSb_2O_6 , and NiSb_2O_6 powders (Fig. 1a–c) can be indexed on the basis of a tetragonal crystal cell. In contrast to $(\text{Co/Ni})\text{Sb}_2\text{O}_6$ that crystallized in the $P4_2/nmn$ space group, CuSb_2O_6 is reported to adopt a lower symmetric $P2_1/n$ space group at ambient temperature, as a consequence of the octahedral distortion due to the presence of Cu^{2+} (d^9).^{8,16} However, the temperature for the monoclinic \rightarrow tetragonal transition is still the subject of some controversies,^{17,18} and our XRD pattern is found to match the tetragonal lattice. Besides the peaks due to this trirutile structure, only a small amount of NiO impurity could be spotted (Fig. 1c). The lattice parameters were refined with the Fullprof software (Table I) and were found to be in good agreement with those reported in the literature.^{8,17–21}

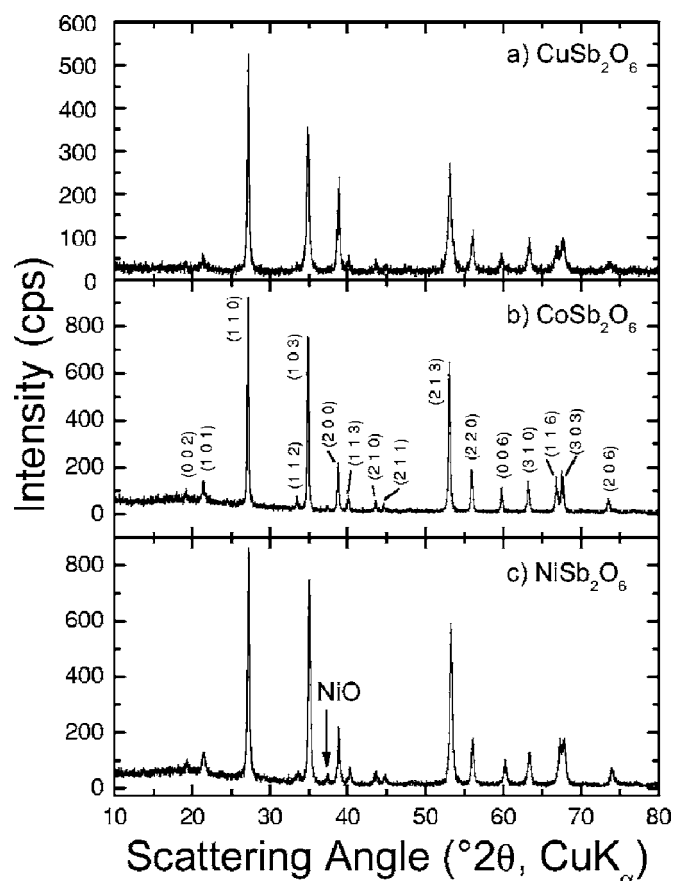


Figure 1. XRD patterns for (a) CuSb_2O_6 , (b) CoSb_2O_6 , and (c) NiSb_2O_6 . These phases having the same structure/space group, Bragg indexing is only displayed for CoSb_2O_6 .

The voltage-composition curves for the first galvanostatic cycles of $\text{MSb}_2\text{O}_6/\text{Li}$ cells are shown in Fig. 2a.

CoSb_2O_6 and NiSb_2O_6 show very similar behavior with a large uptake of about 18–19 Li per formula unit (ca. 1200 mAh/g) through two distinct pseudovoltage plateaus. These large numbers of Li are consistent with the full reduction of the cationic species plus the alloying reaction of Sb with Li leading to Li_3Sb , as is later confirmed by HRTEM, and summarized as



The corresponding derivatives $\delta x/\delta V$ curves (Fig. 2b) exhibit a well-defined peak located at 1.5 V vs $\text{Li}^+/\text{Li}^\circ$ (6–7 Li per formula unit), while the second one (about 12.5 Li per formula unit) is much broader and spread from 1.1 to 0.5 V vs $\text{Li}^+/\text{Li}^\circ$. The length of the first voltage plateau rules out the sole reduction of the M^{2+} cation (2 Li) and it seems difficult to argue a contribution of Li–Sb alloying reaction occurring before the oxide decomposition. Going on, the length of the low-voltage feature (12.5 Li) cannot match the $\text{Sb} \rightarrow \text{Li}_3\text{Sb}$ alloying reaction alone (6 Li) even be associated with the

Table I. Crystallographic parameters for NiSb_2O_6 , CoSb_2O_6 and CuSb_2O_6 .

Sample	Lattice parameters	
	a (Å)	c (Å)
NiSb_2O_6	4.657(2)	9.189(4)
CoSb_2O_6	4.654(3)	9.283(5)
CuSb_2O_6	4.647(6)	9.29(1)

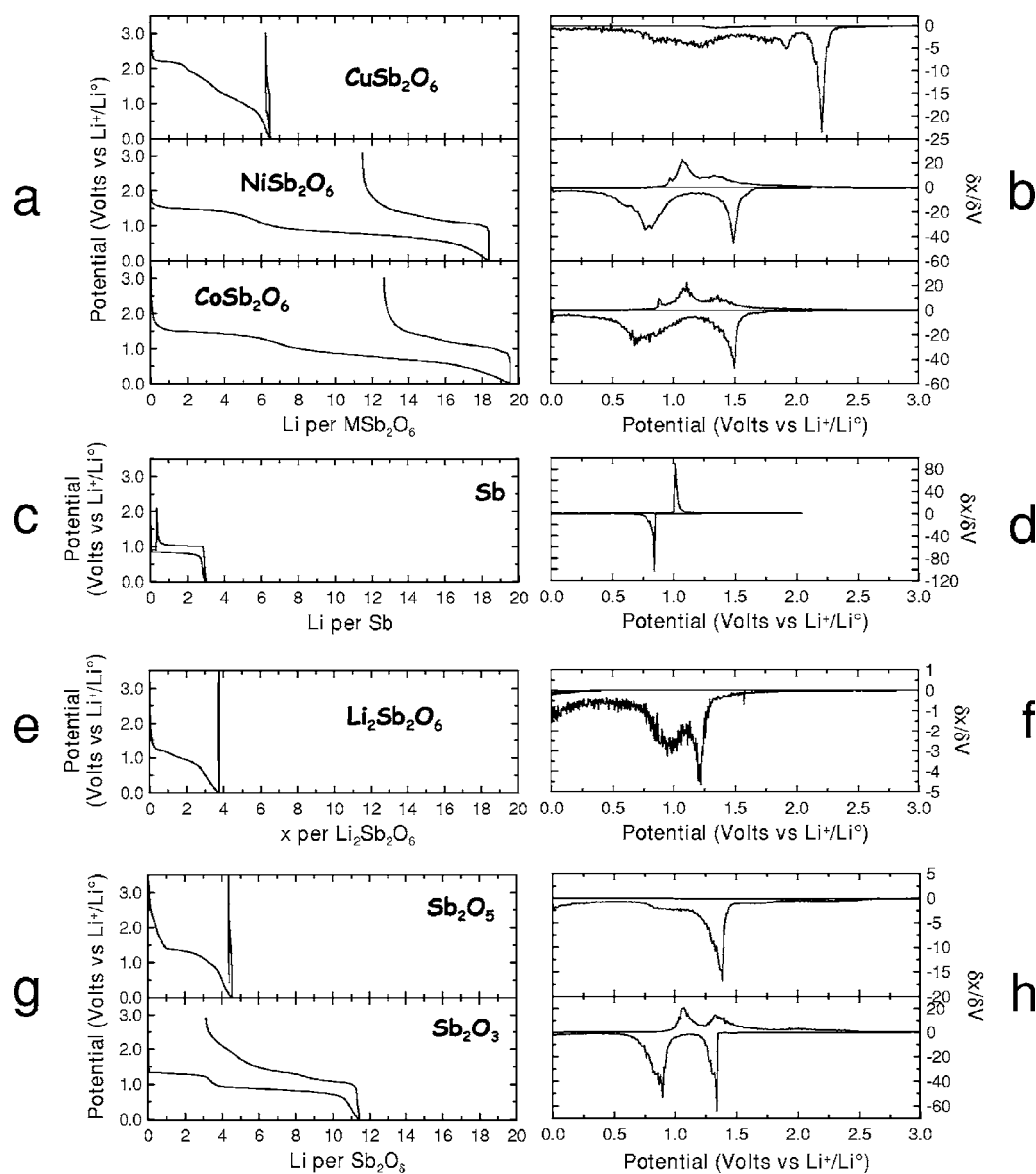


Figure 2. First galvanostatic cycles for various Sb-based materials vs metallic lithium, recorded at 20°C and at a constant current of 1 Li/20 h. (left plots) Voltage-composition curves and (right plots) associated $\delta x/\delta V$ derivatives curves for (a,b) trirutile samples, (c,d) Sb, (e,f) $\text{Li}_2\text{Sb}_2\text{O}_6$, and (g,h) Sb_2O_5 and Sb_2O_3 .

reduction of the M^{2+} species (8 Li). Therefore, the respective capacities observed on these two plateaus cannot be trivially attributed to simple and separated reactions, and the oxide reduction is obviously contributing to both plateaus.

On charge, both CoSb_2O_6 and NiSb_2O_6 materials also behave in a very comparable way with about 7 Li extracted per formula unit through three distinct voltage features: a very small signal at around 0.9 V at the early stage of the process and not identified so far, one broad and intense at 1.1 V, and finally a much broader signal of lower intensity centred at around 1.4 V. From these electrochemical data and comparison with those of a Li/Sb cell (Fig. 2c and d), several comments and observations can be made.

(i) The total absence of charge capacity corresponding to the first discharge reaction (1.5 V) indicates its total irreversibility.

(ii) The voltage of the most intense charge signal (1.1 V) matches that of the $\text{Li}_3\text{Sb} \rightarrow \text{Sb}$ dealloying reaction (see Fig. 2c and d).

(iii) The total capacity associated to the $\text{Sb} \rightarrow \text{Li}_3\text{Sb}$ reaction (0.8 V, Fig. 2c and d) is contributing to the low voltage discharge plateau.

(iv) The high voltage charge reaction (1.4 V) is therefore corresponding to a small fraction of the reaction occurring aside from the alloying process along the low voltage discharge plateau, either a partial re-oxidation of M^0 and/or back formation of Sb-based oxides.

(v) Based on the total charge capacity (7 Li) and on the respective contributions of the 1.1 and 1.4 V reactions, the de-alloying reaction is not totally reversed.

For CuSb_2O_6 , the situation is drastically different (Fig. 2a and b). It reacts with only 6–7 Li on first discharge through a well-defined initial plateau at 2.2 V vs Li^+/Li^0 corresponding to 2 Li per CuSb_2O_6 , followed by a voltage decrease down to 0 V mainly associated with two broad derivative signals at 1.2 and 0.9 V. The subsequent charge surprisingly shows a complete irreversibility of the reaction.

In order to grasp additional data in view of definitive identification of the involved mechanisms, we performed in situ XRD experiments. The evolutions in XRD patterns collected during the discharge of $\text{CoSb}_2\text{O}_6/\text{Li}$ (Fig. 3) and $\text{CuSb}_2\text{O}_6/\text{Li}$ (Fig. 4) cells revealed a complete and progressive amorphization of the materials finally leading to featureless pattern at 0 V. For CoSb_2O_6 , the oxide

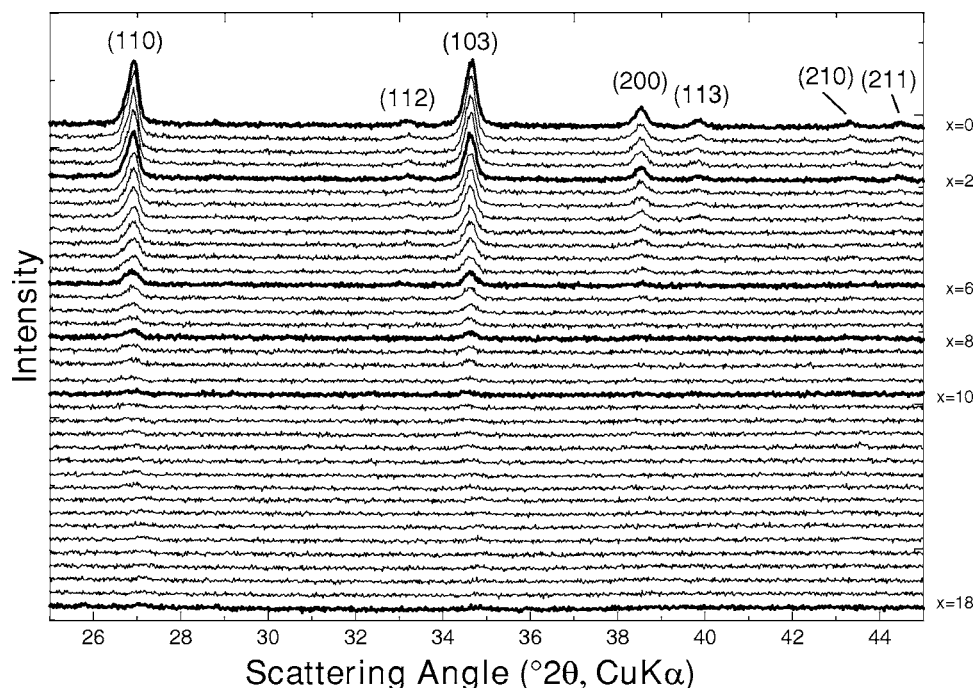


Figure 3. In situ XRD patterns collected on a Li/CoSb₂O₆ cell discharged in a galvanostatic mode at a C/20 rate and at 20°C.

reflections are still vanishing beyond the first plateau (7 Li), confirming the contribution of the oxide decomposition onto both plateaus. When one looks carefully at specific depths of discharge, important differences are spotted (Fig. 5). For instance, at $x = 2$, the reflections due to CuSb₂O₆ are replaced by mainly two slightly shifted and broader peaks. At the same level of reduction, only a slight decrease in reflections intensities is observed for CoSb₂O₆ without any new peak growth or shift. Upon charge after full discharge, XRD patterns are not noticeably changed and only a small amount of unreacted CoSb₂O₆ is detected.

Due to the incapacity for XRD experiments to provide further information about the structural/textural aspects of the electrode materials during discharge, besides its apparent amorphization, we studied both CoSb₂O₆ and CuSb₂O₆ at various stages of their reduc-

tion processes by means of HRTEM. Bright-field images (Fig. 6) indicate that CoSb₂O₆ and CuSb₂O₆ initial materials consist of 100–200 nm and agglomerated 10–50 nm well-crystallized particles, respectively, as deduced from the sharp spots displayed on their corresponding SAED patterns. Note that the smaller size of the CuSb₂O₆ crystallized domains agrees with its broader XRD reflections (Fig. 1). After full reduction, CoSb₂O₆ initial particles transformed into a composite material made of 10–50 nm fairly crystallized Co nanoparticles (Fig. 7a and d) in a matrix of Li₂O and Li₃Sb, as deduced from the line profile of the SAED pattern of the bright-field image (Fig. 7b and c). These observations are in complete agreement with the overall discharge capacity of about 18–19

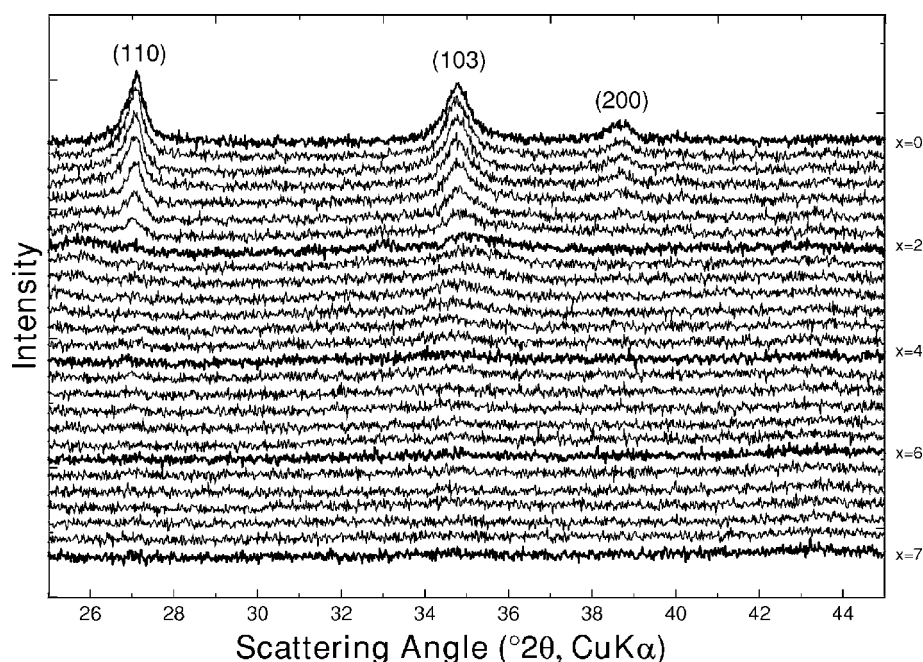


Figure 4. In situ XRD patterns collected on a Li/CuSb₂O₆ cell discharged in a galvanostatic mode at a C/20 rate and at 20°C.

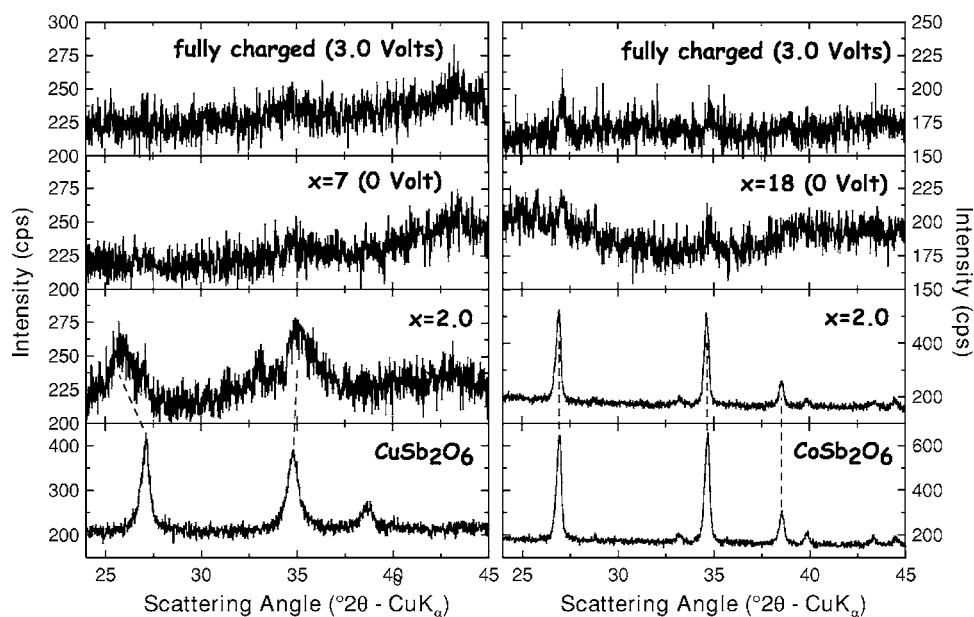


Figure 5. Selected in situ XRD patterns collected along the first galvanostatic cycle for (left panel) Li/CuSb₂O₆ and (right panel) Li/CoSb₂O₆ cells, after reaction of 2 Li per formula unit, full discharge down to 0.0 V, and after full charge at 3.0 V vs Li⁺/Li⁰. In the bottom panels, XRD patterns of the starting materials are displayed for references.

Li/CoSb₂O₆. Similarly to observations made on fully discharged CoO/Li cells,²² the composite agglomerates are surrounded by a thin polymeric-like coating (Fig. 7d).

Similar HRTEM experiments were conducted on fully reduced CuSb₂O₆ (Fig. 8). Bright-field images show the initial particles have transformed into a composite consisting of 5 nm Cu and Sb nanoparticles embedded in an amorphous matrix, as deduced from indexing of SAED patterns. Surprisingly, no trace of Li₂O and/or Li-Sb alloys could be detected. These points were confirmed by heating this discharged material at 350–500°C under inert atmosphere, leading to a mixture of crystallized Cu₂Sb and Sb together with a small amount of Li₂CO₃ likely resulting from the decomposition of residual salts, without any evidence for Li-Sb alloys. Even at 500°C, no crystallization of the matrix occurred.

According to the evolution of the XRD patterns and the peculiar behavior at $x = 2$, HRTEM observations coupled with EDS analyses were conducted at this specific depth of discharge (Fig. 9). It revealed the presence of crystallized Cu nanograins (Fig. 9b), and the Fourier transform of the HRTEM image of the embedding crystallized matrix lead to a reconstructed diffraction pattern very close to

that of the parent CuSb₂O₆ material with only some slight modifications in cell parameters (Fig. 9c), suggesting the following exchange reaction



Interestingly, the formation of ilmenite Li₂Sb₂O₆ through cationic exchange reaction has already been demonstrated.²³ This intermediate formation of a Li₂Sb₂O₆ matrix was confirmed by comparing the electrochemical behavior of CuSb₂O₆ (Fig. 2a and b) with that of a homemade Li₂Sb₂O₆ powder (Fig. 2e and f). Only 4–5 Li per formula unit can be incorporated in this material, while an uptake of 16 Li is expected for its full reduction into a mixture of Li₂O and Li₃Sb. In addition, this small capacity is released through two features corresponding to two broad derivative peaks perfectly matching those observed for a Li/CuSb₂O₆ cell. Finally, the total amount of 6–7 Li reacting per CuSb₂O₆ is in good agreement with the reduction of Cu²⁺ ions followed by the reduction of the as-induced Li₂Sb₂O₆. The nature of the amorphous matrix formed at the bottom of this discharge being still out of reach, we collected the

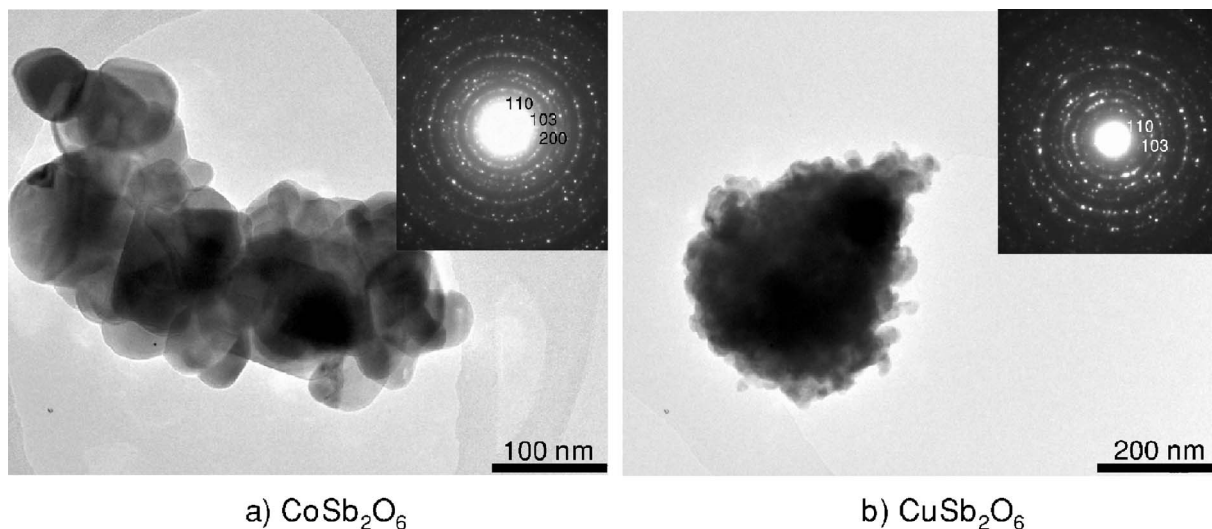


Figure 6. Bright-field TEM images for (a) CoSb₂O₆ and (b) CuSb₂O₆ powders with (insets) corresponding indexed SAED patterns.

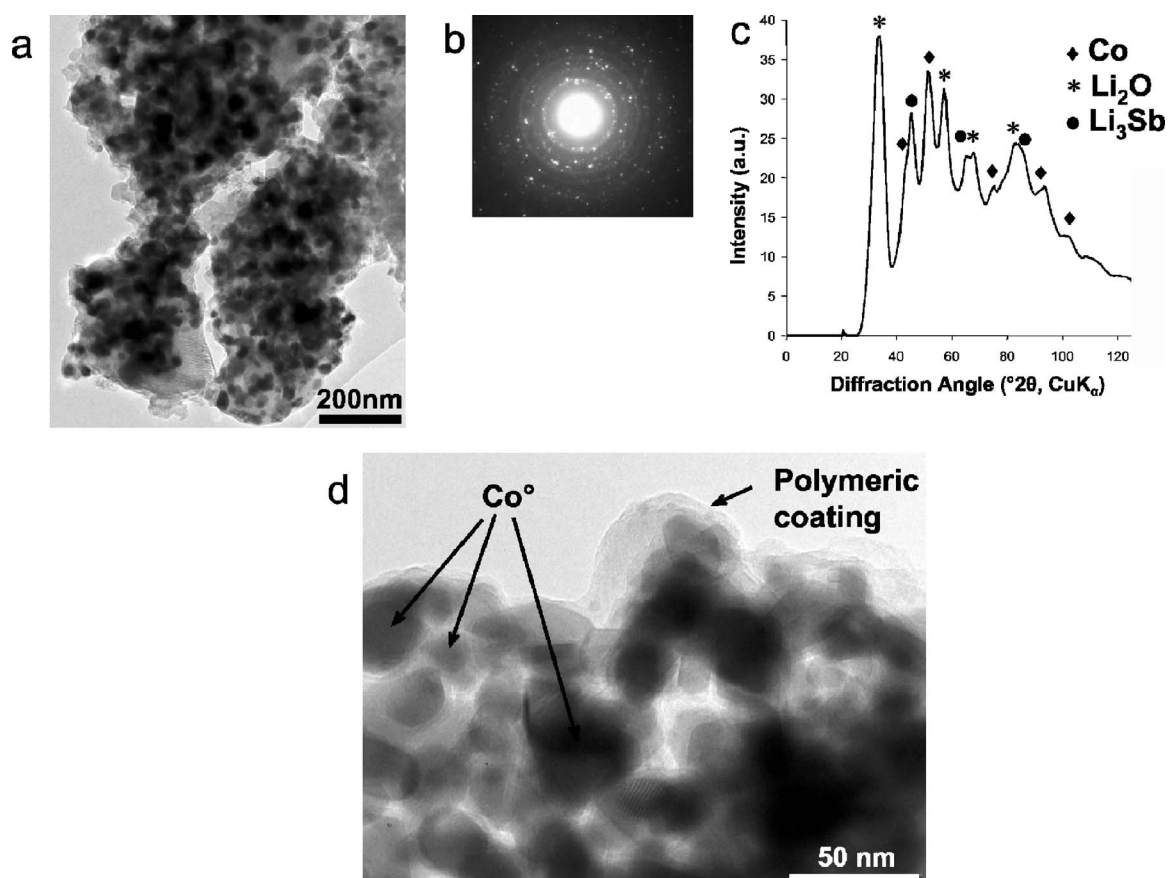


Figure 7. (a) Bright-field TEM and (d) HRTEM images, (b) corresponding SAED pattern, and (c) phase composition as deduced from indexation of the SAED pattern, for a powder recovered after full discharge (18 Li per formula unit, 20°C) of a Li/CoSb₂O₆ cell.

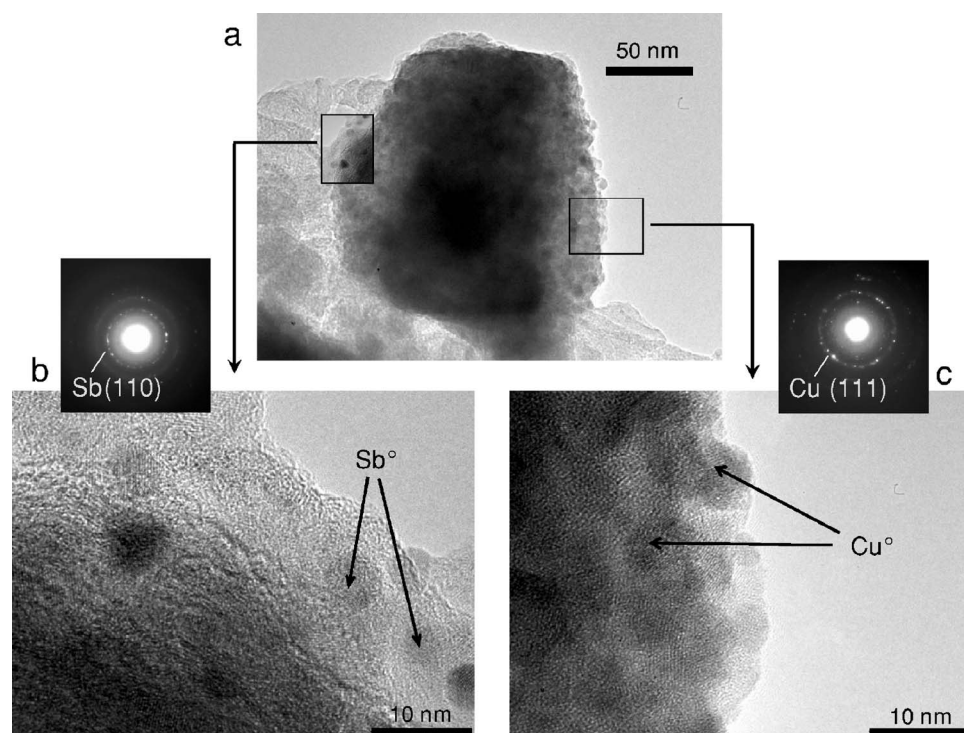


Figure 8. (a) Bright-field TEM images and (b,c) SAED patterns and HRTEM images showing the presence of both Cu° and Sb° metals, for the powder recovered after full discharge (7 Li per formula unit, 20°C) of a Li/CuSb₂O₆ cell.

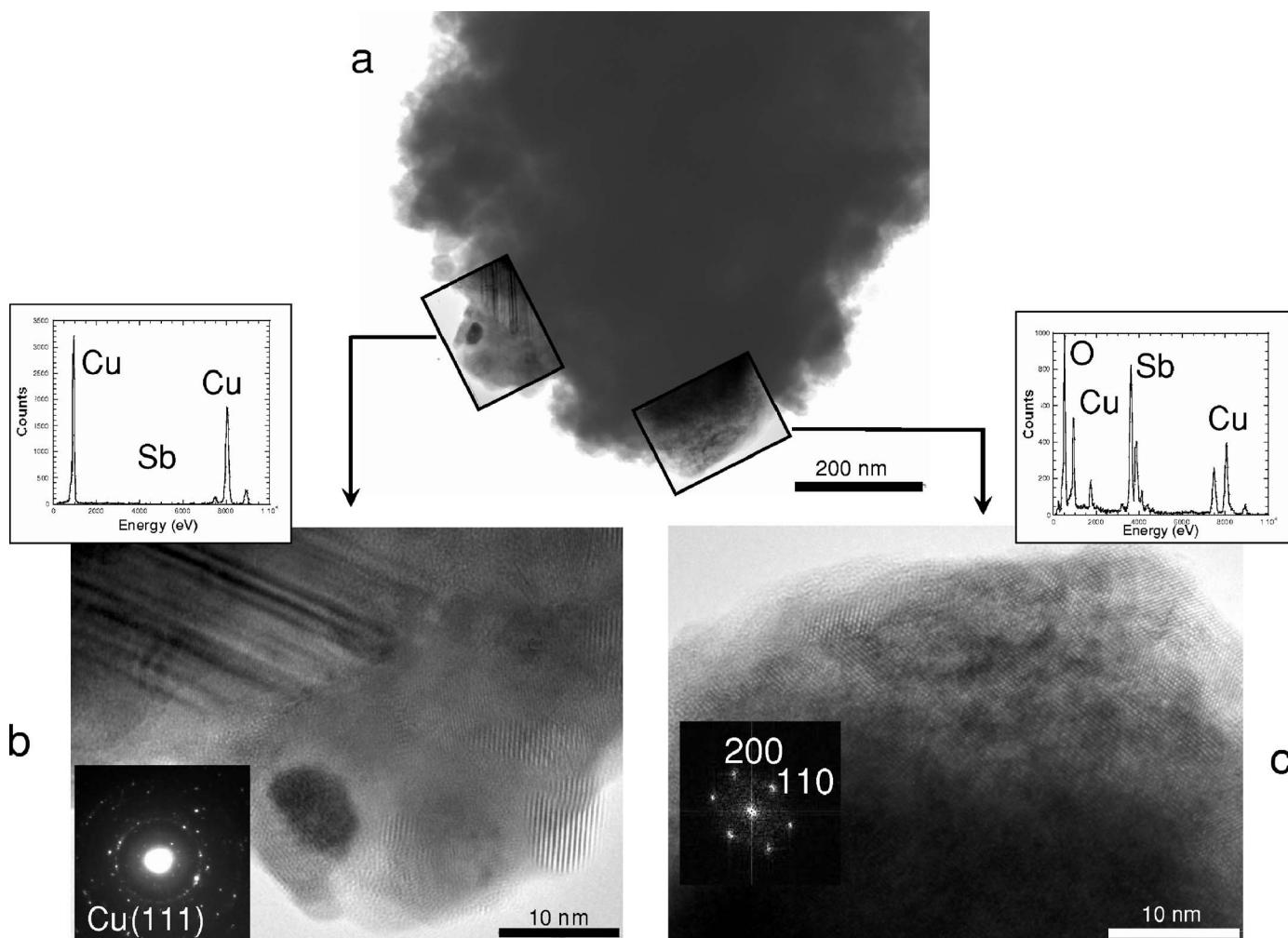


Figure 9. (a) Bright-field TEM image and (b,c) two selected HRTEM pictures with corresponding EDS spectra and either indexed SAED pattern or reconstructed electron diffraction pattern obtained by Fourier transform of the bright-field image, for the powder recovered after partial discharge (2 Li per formula unit, 20°C) of a Li/CuSb₂O₆ cell.

Mössbauer signal. As shown on Fig. 10 and Table II, about half of the antimony (43%) is still at the +V state after full discharge (Fig. 10c), and very similar Sb^V contents (46%) were measured for fully

reduced LiSbO₃ (Li₂Sb₂O₆) (Fig. 10a). Interestingly, for a fully discharged CuSb₂O₆/Li cell, aside from the Sb⁰ Mossbauer signal

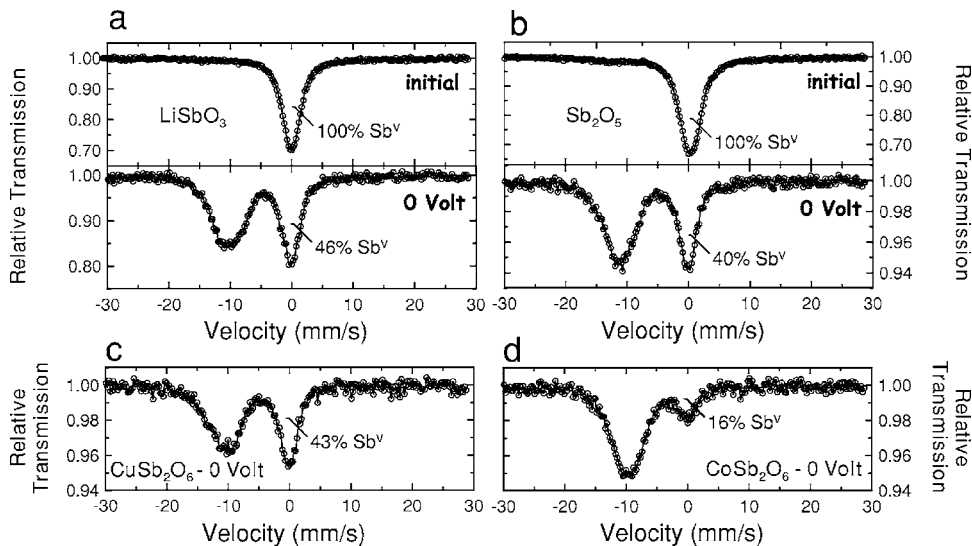


Figure 10. Mössbauer spectra for (a) initial and reduced LiSbO₃ at 0.0 V, (b) initial and reduced Sb₂O₅ at 0.0 V, (c) reduced CuSb₂O₆ at 0.0 V, and (d) reduced CoSb₂O₆ at 0.0 V. Discharge of the cells was done at 20°C and at a 1 Li/20 h rate. Spectra were collected at 4 K and the zero isomer shift was defined from the spectrum of InSb at 4 K [$\delta = -8.70(4)$ mm/s relatively to the Ba^{121m}SnO₃ source].

Table II. ^{121}Sb Mössbauer data for initial LiSbO_3 , Sb_2O_5 , CuSb_2O_6 , CoSb_2O_6 and after reduction down to 0.0 V vs $\text{Li}^+/\text{Li}^\circ$ (20°C). δ = isomer shift relative to InSb (−8.70 mm/s relatively to $\text{Ba}^{121\text{m}}\text{SnO}_3$ source), Δ = quadrupole splitting, Γ = line width, X^2 = chi-squared, and Misfit = comparative goodness of fit criterion which gives the fraction of the experimental signal that remains unfitted.

Sample	δ (mm/s)	Δ (mm/s)	Γ (mm/s)	C (%)	X^2	Misfit (%)	Ref.
LiSbO_3	+8.69(1)	—	1.28(2)	100	1.41	0.07	^a
LiSbO_3	−0.28(6)	+10.2(9)	1.46(5)	28	1.14	0.07	^a
0 V	−3.02(6)	+8.9(7)	1.46(5)	26			
	+8.58(1)	—	1.46(5)	46			
Sb_2O_5	+9.04(1)	—	1.63(2)	100	2.88	0.19	^a
Sb_2O_5	−1.3(4)	+11(4)	1.42(6)	26	1.14	0.11	^a
0 V	−3.7(1)	+13(1)	1.42(6)	34			
	+8.61(2)	—	1.42(6)	40			
CuSb_2O_6	+8.8	+1.3	—	100			17
CuSb_2O_6	−0.45(7)	+5(1)	1.51(2)	27	0.96	0.17	^a
0 V	−3.5(1)	+13(1)	1.51(2)	30			
	+8.55(2)	—	1.51(2)	43			
CoSb_2O_6	+8.6	+2.7	—	100			17
CoSb_2O_6	+0.39(8)	+7(1)	1.98(2)	37	1.06	0.08	^a
0 V	−2.27(7)	+10.2(9)	1.98(2)	47			
	+8.64(5)	—	1.98(2)	16			

^a This work.

(30%, $\delta = -3.5$ mm/s),²⁴ another contribution at $\delta = -0.45$ mm/s (27%) may match intermetallic phase such as Cu_2Sb , clueing some interaction between the two expelled metals. This intimate metal mixing could also account for the easy formation of crystallized intermetallics upon mild heating, as previously described. From all these results, the complete reaction of Li with CuSb_2O_6 leads to the formation of a mixture of nano-Sb and Cu particles expelled from, and embedded in, an amorphous $\text{Li-Sb}^{\text{V}}\text{-O}$ matrix, summarized as follows



This scenario implies that the Sb particles are not able to undergo any alloying reaction with Li at low voltage, suggesting an ionic and/or electronic isolating role of the $\text{Li-Sb}^{\text{V}}\text{-O}$ matrix. Actually, the lithium-rich Sb^{V} oxides are well known to be very fast ionic conductor materials,²⁵ and many reports indicated very poor electron conduction and large bandgap for Li-containing $\text{Sb}^{\text{V}}\text{-based}$ ox-

ides, some being even used as dielectric additives.²⁶⁻²⁸ In addition to the composition of the composite recovered at the bottom of the discharge (Cu/Sb metals and $\text{Sb}^{\text{V}}\text{-based}$ matrix), this electronic isolating effect can explain the total absence of charge capacity. Back to $(\text{Co/Ni})\text{Sb}_2\text{O}_6$, the fully discharged material was confirmed by Mössbauer to have a limited 16% Sb^{V} content (Fig. 10d, Table II), confirming the large extent of the reaction up to the alloying reaction.

The conductivity issue can also be illustrated by the evolutions in the OCV and GITT traces, compared in Fig. 11. The polarization of a $\text{Li/CuSb}_2\text{O}_6$ cell (Fig. 11a) slowly decreases during the reaction with the first 2 Li, consistently with the in situ formation of metallic Cu acting as a conductive additive. Then, beyond this point, the polarization continuously increases (up to about a value of 1.2 V), as expected for the continuous formation of an isolating Li-rich $\text{Sb}^{\text{V}}\text{-O}$ matrix. Worth being pointed out is the absence of constant

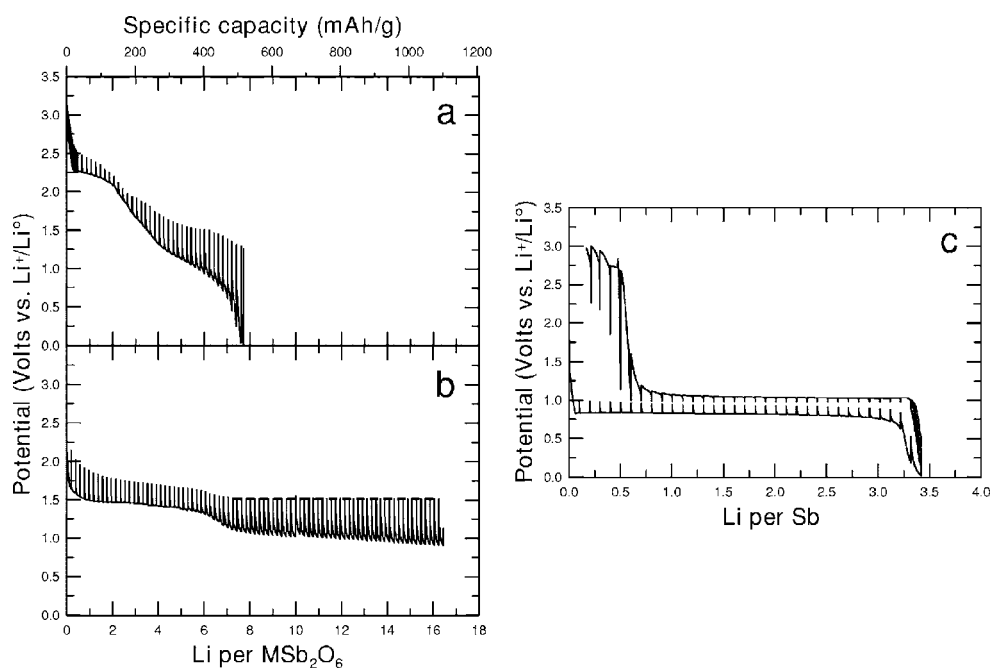


Figure 11. Voltage-composition curves in GITT mode (1 Li/10 h, 20°C) for (a) $\text{Li/CuSb}_2\text{O}_6$, (b) $\text{Li/CoSb}_2\text{O}_6$, and (c) Li/Sb cells. The quasiequilibrium OCVs were recorded when the time evolution of the voltage was lower than 3 mV/h.

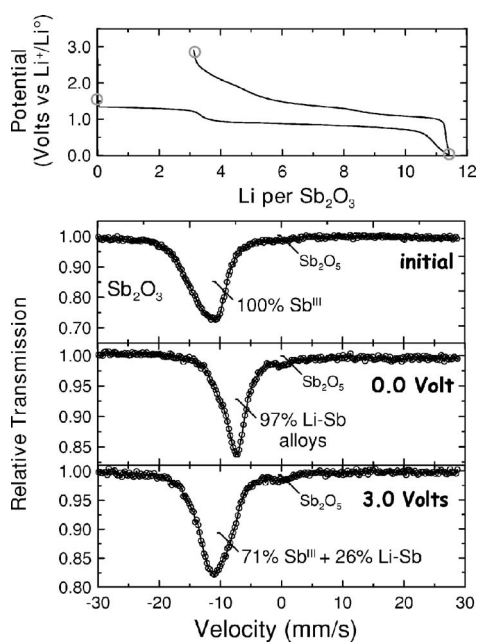


Figure 12. (top panel) First galvanostatic cycle for a Li/Sb₂O₃ cell (20°C, 1 Li/20 h) and (bottom panel) selected Mössbauer spectra. Spectra were collected at 4 K and the zero isomer shift was defined from the spectrum of InSb at 4 K [$\delta = -8.70(4)$ mm/s relatively to the Ba^{121m}SnO₃ source].

OCV ranges, generally cluing biphasic domain such as Li–Sb alloying reaction (Fig. 11c). For a Li/CoSb₂O₆ cell (Fig. 11b), the polarization is roughly constant during the first plateau (about 6 Li in length) while it slightly and progressively increases along the second one while still remaining far smaller than values measured for a Li/CuSb₂O₆ cell. Beyond this value of 6 Li reacted, the perfectly constant OCV values indicate at least one biphasic process.

By looking at the reactivity of Li with Sb₂O₅ and Sb₂O₃ and associated derivative curves (Fig. 2g and h), it is clear that (Co/Ni)Sb₂O₆ behaves as a trivalent oxide and that the short capacity and complete irreversibility noted for Sb₂O₅ mimic the behavior of Li₂Sb₂O₆ and CuSb₂O₆. For both binary oxides, the first discharge voltage plateau is still found totally nonreversible, and amorphous materials were formed at bottom discharge as deduced from in situ XRD measurements. Mössbauer analyses further confirmed the similarity with Cu-based trirutile with a large amount of remaining unreduced Sb^V (40%) for fully discharged Li/Sb₂O₅ cells (Fig. 10b). For a Li/Sb₂O₃ cell, Mössbauer spectra showed the complete transformation at 0.0 V into mainly Li₃Sb alloy ($\delta =$

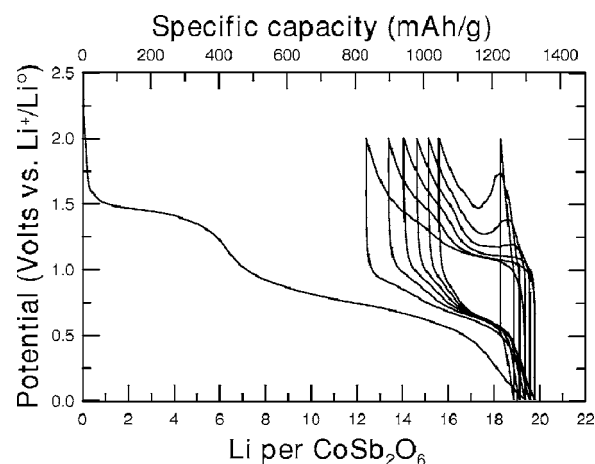


Figure 14. Cycling galvanostatic voltage-composition curve (1 Li/20 h, 20°C) for a Li/CoSb₂O₆ cell. Beyond the third cycle, note the temporary increase in polarization on charge.

-0.45 mm/s),²⁴ and the partial back formation of trivalent oxide (71%) which amount is totally consistent with the charge capacity recovered at 3.0 V (Fig. 12, Table III). The effect of the Sb oxidation state could also be illustrated by the drastic increase in capacity on the lower discharge plateau and therefore improvement of the charge reversibility when moving from Sb₂O₅ to Sb₂O₄ (Sb^{III}, Sb^V) by a simple air-heating treatment (Fig. 13). The same trends were noticed by Courtney et al. for amorphous Sb–O-based glasses with various Sb/O ratios.²⁹ By the way, the complete irreversibility noted for Li/Sb₂O₅ cell rules out the formation of Sb₂O₅ + Ni⁰ at the early stage of the reduction of (Co/Ni)Sb₂O₆.

The first reduction step for (Co/Ni)Sb₂O₆ is thus believed to consist in the reduction of pentavalent antimony, while that of CuSb₂O₆ leads to Li₂Sb₂O₆ and finally isolating Li–Sb^V–O. The intimate process linked to this aspect and the specific role of the divalent metal are still not fully understood, but this point is presently being studied by in situ Mössbauer spectroscopy.

Finally, despite the very small size of the Sb and Sb alloys formed during the first discharge, the long-term cycling behavior of (Co/Ni)Sb₂O₆ (2,0–0,0 V) was not satisfactory. After a few cycles, the voltage-composition curve developed an uncommon large and temporary rise in polarization at the early stage of the charge and was responsible for the final drop in capacity (Fig. 14). This point has not been figured out so far but an overlapping of the charge processes (dealloying plus back formation of oxides) may result in a complex sequence of reactions and evolving conductivity.

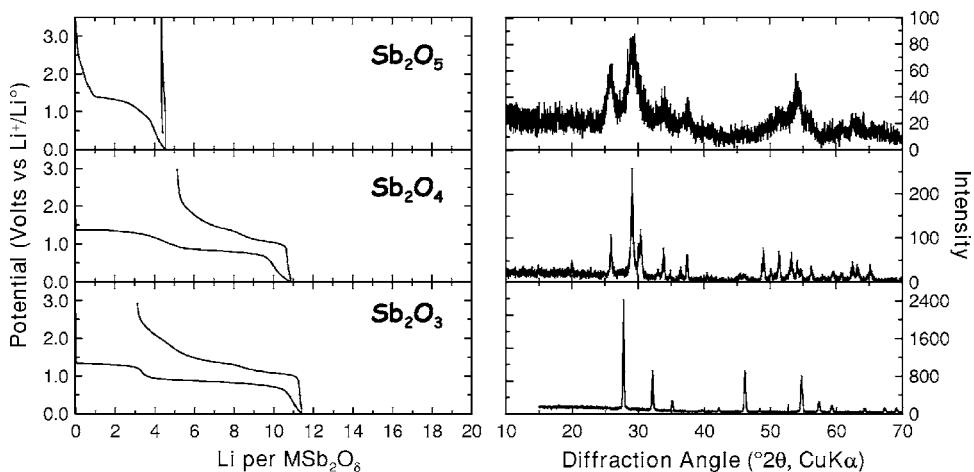


Figure 13. (right panel) XRD patterns for Sb oxides with various metal oxidation states, and (left panel) corresponding first galvanostatic cycles vs Li⁰ (20°C, 1 Li/20 h).

Table III. ^{121}Sb Mössbauer data for initial Sb_2O_3 , after reduction down to 0.0 V and after subsequent oxidation at 3.0 V vs $\text{Li}^+/\text{Li}^\circ$ (20°C). δ = isomer shift relative to InSb (−8.70 mm/s relatively to $\text{Ba}^{121\text{m}}\text{SnO}_3$ source), Δ = quadrupole splitting, Γ = line width, X^2 = chi-squared, and Misfit = comparative goodness of fit criterion which gives the fraction of the experimental signal that remains unfitted.

Sample	δ (mm/s)	Δ (mm/s)	Γ (mm/s)	C (%)	X^2	Misfit (%)
Sb_2O_3	−3.38(1)	+18.3(1)	1.63(3)	100	1.85	0.11
Sb_2O_3	+1.57(2)	—	1.47(5)	65	1.19	0.05
0 V	−0.50(5)	+10.9(5)	1.47(5)	32		
	+9.0(2)	—	1.47(5)	3		
Sb_2O_3	−2.89(2)	+10.0(2)	1.68(1)	71	1.12	0.03
3.0 V	+0.1(1)	—	1.68(1)	26		
	+8.9(2)	—	1.68(1)	3		

Conclusions

The electrochemical reactivity of MSb_2O_6 ($\text{M} = \text{Cu}, \text{Ni}, \text{Co}$) phases with Li were investigated in order to understand their potentiality as negative electrodes. The study revealed drastically different behaviors and reaction mechanisms depending on the nature of the divalent ion. While CuSb_2O_6 reacts with only 6–7 Li during the first discharge and there is no subsequent charge capacity, NiSb_2O_6 and CoSb_2O_6 react with 18–19 Li and 6 Li could be removed on first cycles. By coupling electrochemical analyses with in situ XRD measurements and HRTEM/Mössbauer data, we could propose a scenario accounting for these surprising redox behaviors. The reduction of CuSb_2O_6 proceeds via a two-step process initially involving the expulsion of metallic copper clusters, leading to amorphous pentavalent $\text{Li}_2\text{Sb}_2\text{V}_2\text{O}_6$ that can secondly further react with Li by expulsion of metallic nano-Sb embedded in the resulting Li-rich $\text{Li}_7\text{Sb}_2\text{V}_2\text{O}_6$ amorphous pentavalent matrix. The high electronic insulating effect of this matrix prevents alloying of Li with extruded Sb and causes the complete irreversibility of the reaction. In contrast, $(\text{Co}/\text{Ni})\text{Sb}_2\text{O}_6$ are totally reduced into a mixture of Li_2O , Co/Ni , and Li_3Sb and partial reversibility is thus recovered. A close parallel can be made between these results and the compared reactivity of Sb_2O_5 and Sb_2O_3 , suggesting that the nature of the divalent cationic species plays a crucial role in determining the nature and oxidation state of the intermediates phases formed along the first discharge, directly determining the charge yield. The present study exemplified that reduction process and therefore cycling performances in the Li–Sb–O system can be drastically and unexpectedly altered by the initial oxidation state of Sb and by its evolution upon first reduction. Although not exhibiting satisfactory cycling behavior, many aspects of the reactivity of these binary and ternary materials are still questioned and worth further investigations.

Université de Picardie Jules Verne assisted in meeting the publication costs of this article.

References

- P. Poizot, S. Laruelle, S. Grugeon, L. Dupont, and J. M. Tarascon, *Nature (London)*, **407**, 496 (2000).
- D. Larcher, C. Masquelier, D. Bonnin, Y. Chabre, V. Masson, J.-B. Leriche, and J.-M. Tarascon, *J. Electrochem. Soc.*, **150**, A133 (2003).
- P. Balaya, H. Li, L. Kienle, and J. Maier, *Adv. Funct. Mater.*, **13**, 621 (2003).
- N. Pereira, L. C. Klein, and G. G. Amatucci, *J. Electrochem. Soc.*, **149**, A262 (2002).
- H. Li, G. Richter, and J. Maier, *Adv. Mater. (Weinheim, Ger.)*, **15**, 736 (2003).
- R. Alcantara, J. L. Tirado, J. C. Jumas, L. Monconduit, and J. Olivier-Fourcade, *J. Power Sources*, **109**, 308 (2002).
- P. Poizot, S. Laruelle, S. Grugeon, and J. M. Tarascon, *J. Electrochem. Soc.*, **149**, A1212 (2002).
- A. Bystrom, B. Hock, and B. Mason, *Ark. Kemi, Mineral. Geol.*, **B15**, 1 (1941).
- W. Weppner and R. A. Huggins, *J. Electrochem. Soc.*, **125**, 7 (1978).
- P. S. Gopalakrishnan and H. Manohar, *Cryst. Struct. Commun.*, **4**, 203 (1975).
- W. Gruender, H. Paetzold, and H. Strunz, *Neues Jahrb. Mineral., Monatsh.*, **1962**, 93–8.
- J. Rodriguez-Carvajal, *Physica B*, **192**, 55 (1993).
- M. Morcrette, Y. Chabre, G. Vaughan, G. Amatucci, J.-B. Leriche, S. Patoux, C. Masquelier, and J.-M. Tarascon, *Electrochim. Acta*, **47**, 3137 (2002).
- K. Rubenbauer and T. Birshall, *Hyperfine Interact.*, **7**, 125 (1979).
- J. L. Lábár, *Microscopy and Analysis*, **75**, 9 (2002) (Euro. edit.).
- V. Propach and D. Reinen, *Z. Anorg. Allg. Chem.*, **369**, 278 (1969).
- J. D. Donaldson, A. Kjekshus, D. G. Nicholson, and T. Rakke, *Acta Chem. Scand., Ser. A*, **A29**, 803 (1975).
- E.-O. Giere, A. Brahimi, H. J. Deiseroth, and D. Reinen, *J. Solid State Chem.*, **131**, 263 (1997).
- J. N. Reimers, J. E. Greedan, C. V. Stager, and R. Kremer, *J. Solid State Chem.*, **83**, 20 (1989).
- A. M. Nakua, H. Yun, J. N. Reimers, J. E. Greedan, and C. V. Stager, *J. Solid State Chem.*, **91**, 105 (1991).
- A. M. Nakua and J. E. Greedan, *J. Cryst. Growth*, **154**, 334 (1995).
- M. Dolle, P. Poizot, L. Dupont, and J.-M. Tarascon, *Electrochem. Solid-State Lett.*, **5**, A18 (2002).
- N. Kumada and K. Nobukazu, *Mater. Res. Bull.*, **28**, 849 (1993).
- L. Aldon, A. Garcia, J. O. Fourcade, J. C. Jumas, F. J. F. Madrigal, P. Lavela, C. P. Vicente, and J. L. Tirado, *J. Power Sources*, **119**, 585 (2003).
- C. Muehle, R. E. Dinneber, L. van Wuelen, G. Schwering, and M. Jansen, *Inorg. Chem.*, **43**, 874 (2004).
- H. Boursset, P. Salles, and J.-M. Savariault, *Solid State Ionics*, **106**, 315–320 (1998).
- J. M. S. Skakle, M. A. Castellanos, R. S. T. Tovar, and A. R. West, *J. Solid State Chem.*, **131**, 115 (1997).
- W. W. Coffeen, *J. Am. Chem. Soc.*, **39**, 154 (1956).
- I. Courtney, Ph.D. Thesis, Dalhousie University, Halifax, Nova Scotia, Canada (1999).